

Investigating the Thermionic Effect of Broken Perforated Curved Ribs on Solar Preheater Through Cfd Simulation

By

Shivasheesh Kaushik

Assistant Professor, Department of Mechanical Engineering, Shivalik College of Engineering, Dehradun

Email: shivasheeshkecua@gmail.com

Kuldeep Panwar

Associate Professor, Department of Mechanical Engineering, Shivalik College of Engineering, Dehradun

Samriddhi Vashisth

Scholar, Department of Mechanical Engineering, Shivalik College of Engineering, Dehradun

Abstract

By utilising absorber plates exposed to solar radiation, solar air warmers efficiently harness solar energy. The absorbed radiation is next converted into thermionic energy at periphery of plates, and ultimately the thermionic energy is transported to fluid that is carried via a collector. The fact that there is little convective heat transfer amidst at absorber plate and air absorbs the heat while flows over it. Demonstrate's low efficiency of flat plate solar preheaters. Most popular and efficient way to increase a solar preheater effectiveness is to incorporate roughness (broken perforated curve ribs) absorber plate features from the bottom half. The research's central idea is a solar preheater with purposefully roughened, broken perforated curved ribs that predict the device's convective heat transmission characteristics. A useful tool for heating a space using photovoltaic energy is a solar preheater. A Reynolds no. (Re) can be amidst 4000 and 20,000. This aims to derive comparative analysis of perforated roughness parameters like roughness height (e/D_h), comparative roughness pitch (8–14), comparative roughness curve angle (30–75), comparative roughness curve hydraulic dia (0.0333 metres), and comparative roughness width gap ($g/e=1$)—broken curved roughness of the 5:1 aspect ratio solar preheater absorber plate. The simulations of computational fluid dynamics (CFD) were performed using ANSYS FLUENT 15.0 programme. Similar flow parameters and outcomes of smooth passage are compared with other roughned passage. Computational fluid dynamics (CFD) simulations used to perform ANSYS FLUENT 15.0 programme. Outcome's of the smooth passage (duct) and roughned passage (duct) are compared to the impact of different parameters on heat transmission and friction when the flow conditions are same.

Index Terms: Solar Preheater, unnatural roughness, broken curved ribs, and Ansys 14.5.”

1. Introduction

As it is anticipated that conventional resources would run out in the next years, as rising cost of energy has led many individuals to think about alternative and renewable energy sources. These days, a variety of resources are available, including tidal, wind, solar, and bio-gas. The most accessible source is solar which can heat homes in the winter, light homes, and preparing meals. Solar energy from a Solar Preheater is transformed into Thermionic energy. This thermionic energy can warm up spaces, dry clothes, cultivate crops, and complete a no.

of other tasks. Since they have an easy-to-understand construction and with low little effort and money to install, air heaters are frequently used. Despite the fact that conventional Solar Preheater have a low heat transfer coefficient amidst absorber plate and flowing air due to the formation of a laminar sub-layer turbulent boundary layer next to the absorber plate's heat transfer surface, Thermionic efficiency is still low in turbulent conditions. This is because laminar sub-layer is side-by-side to heat transmission layer of absorber plate. When thickness of laminar sub-layer increased in direction of flow, the thermionic performance of common Solar Preheater declines.

Multiple methods, such as duplicate passes, finned absorbers, packed beds, periodic rib roughness, and others, are combined to enhance thermionic performance. The periodic rib roughness technique ultimately the successful performance enhancement method because, in contrast to the other methods, it generates turbulence in a flow zone near the heat-transfer boundary of the absorber layer without affecting the core flow. This causes a laminar sub-layer to form in this flow zone. The method now stands out from the competitors as a result. The necessary pumping force decreases as a result.

Solar preheater duct that had been purposely roughened by v.s. was used in this investigation to evaluate the relationships amidst heat transmission and friction factor. During this experimental examination, Hans and his colleagues looked at a solar preheater duct with a 12-aspect ratio that had been roughened by a broken arc rib. Researchers studied a roughened plate of comparative roughness parameters ranging from 4° to 75° for comparative roughness pitch (P/e), relative gap width (g/e), comparative gap position (d/w), comparative roughness height (e/Dh), and comparative arc angle (θ). The goal of this research was to determine how this roughness parameter alters Nusselt no. and friction factor.

The greatest increases in Nusselt no. and friction factor 1,19 and 1,14 times excess in a continuous arc rib roughened duct, respectively. The equivalent outcomes were 2,63 and 2,44 times better than what may have been predicted from a smooth tube, respectively. In order to conduct this study, a computer analysis of the heat transmission and functional properties of a rectangular solar preheater duct with semi-elliptical obstacles was performed. The title of the essay is "Numerical research on thermionic hydraulic performance enhancement in solar preheater duct with semi-ellipse shaped obstacles," and its author is Tabish Alam. Renormalization-group k-turbulence replica simulations in three dimensions have been carried out. Attack angle in V-down arranged obstacles on the absorber plate lies between 30 to 90 degrees. On opposite side thought as of viable choices are the staggered and inline obstacle patterns. The Nusselt no. and friction factor were calculated by using four alternative Reynolds values, ranging from 6000 to 18000. The Nusselt no. and the friction factor are highly influenced by the angle of attack, represented by α , and the position of the barriers.

The maximum enhancements in Nusselt no. and friction factor in a staggered design were calculated to be 2.05 and 6.93, respectively, as opposed to 1.73 and 6.12 for an inline configuration. The angle of attack of 75 degrees causes the Nusselt no. to climb the most. This is because this angle of attack results from the interaction amidst high turbulence and lateral air flow movement. For all values of the attack angle evaluated in this study, the results of the

thermionic-hydraulic performance analysis indicate that staggered layouts outperform inline arrangements on all fronts. A/c, Tabish Alam's critical assessment of unnatural roughness provided in rectangular solar preheater ducts, applications of unnatural roughness on the underside of the absorber plate in solar preheater ducts are widely used to enhance heat transfer with only a modest increase in friction factor. Optimizing surfaces that have undergone a roughening treatment requires careful planning of the shape and distribution of the roughness. The flow structure, which is governed by the roughness factors and the rib shape, determines how heat is transmitted. A thorough analysis of the several different unnatural roughness elements described in the literature is followed by a investigation of the effects of the diverse roughness patterns. . It has been determined that it is a link amidst the Nusselt no. and the friction factor for various roughness components. A comparative evaluation of the thermionic-hydraulic completion of various roughness components has also been provided as part of the effort to get a deeper comprehension of the consequences of unnatural roughness.

The thermo-hydraulic performance of an absorber plate with recognisable hyperbolic ribs of roughness height (e) ranging from 0.5 mm to 2 mm and pitch (P) varying from 10 mm to 20 mm was evaluated by Deep Singh Thakur et al. [4] using a CFD analysis. The roughness height was amidst 0.5 and 2 mm. The best performance can be attained by keeping the Re value at 6000 while setting $e = 1$ mm and $P = 10$ mm. It is shown that this particular rib works the best up to $Re = 100,000$ compared to rectangular, triangular, and semicircular rib shapes.

Amit Kumar Ahuja et al. [5] employed a CFD replica to examine the thermo-hydraulic performance of a synthetically roughened solar absorber plate. The plate had a homogeneous heat flux of 1000 w/m², a hydraulic diameter of 33.33, and a Reynolds no. of 8000-180000. 7.14–20 was the comparative roughness pitch, and 0.03-0.042 was comparative roughness height. A rise in the normal Russell no. results from an increase. On absorbering layer of solar preheater, N.K., were several arcs with gaps. This was done to achieve the highest possible assess heat transmission. Pandey et al. [6] included following parameter's in their study: comparative roughness height (e/D) values amidst 0.016 and 0.044 (4 values), comparative roughness pitch (p/e) values amidst 4 and 16 (4 values), arc angle values amidst 30-75 (4 values), comparative roughness width (W/w) values amidst 1 and 7 (5 values), and comparative gap distance (d/x) values amidst 0.25 and 0.85 (4 values). (4 values). Several arcs with gaps could be seen on the absorber plate of the solar preheater, N.K. The goal of doing this was to maximise the rate of heat transport. All of the parameters listed below were included in the study by Pandey et al. [6]: comparative roughness height (e/D) values amidst 0.016 and 0.044 (4 values), comparative roughness pitch (p/e) values amidst 4 and 16 (4 values), arc angle values amidst 30-75 (4 values), comparative roughness width (W/w) values amidst 1 and 7 (5 values), and comparative gap distance (d/x) values amidst 0.25 and 0.85. (4 values). 4 values. Nusselt no. (Nu) and friction factor (f) climb by 5.85 and 4.96 times, respectively, which are the largest increases, as compared to a smooth duct. The maximal enhancement of Nu is produced by values of 21,000 for the Reynolds no. (Re), 1 for the g/e ratio, 0.65 for the d/x ratio, 5 for the W/w ratio, 0.044 for the e/D ratio, 8 for the p/e ratio, and 1 for the $a/60$ ratio. Yadav and Bhagoria utilised CFD to examine the effects of heat transmission and flow of fluid characteristics in a solar preheater that had been intentionally roughened. The movement of fluid and the transfer

of heat have both been studied in relation to the roughness of the transverse wire ribs. It was discovered that at a comparative roughness pitch of 7.14 and a comparative roughness height of 0.042, the standard Nusselt no. at a higher Reynolds no. of 18,000 had a maximum value of 117. At a comparative roughness pitch of 7.14 and a comparative roughness height of 0.042, this was the situation. The standard Nusselt no. and frictional factor increased the most in comparison to a smooth duct at a comparative roughness pitch of 7.14 and a comparative roughness height of 0.042, respectively. Comparing this enhancement to a smooth duct, it was 2.31 times and 0.0317 times greater.

In addition to determining the friction factor amidst a discretized broken V-pattern baffle solar air channel, Raj Kumar et al. also explored and produced the Nusselt no.. The comparative baffle height, which ranges from 0.25 to 0.80, the comparative baffle pitch, which ranges from 0.5 to 2.5, and the angle of attack, which ranges from 30 to 70 degrees, have all been determined through experiments. The comparative baffle gap distance, which ranges from 0.26 to 0.83, the comparative baffle gap width, which ranges from 0.5 to 1.5, and the comparative baffle height have also all been determined. Furthermore, the impact of a discretized broken V-pattern baffle has been studied in the Reynolds no. range of 3000 to 21000. The angles of 0.67, 1.0, 0.50, 1.5, and 60 degrees may have the highest elevation increase. The emphasis in earlier literature was on thermionic and performance investigation based on the use of geometrical structures influenced by unnatural roughness [26, 29, 36, 38], various geometrical shapes over solar plates [26, 29, 36, 38], diverse heat pipe designs with or without fins/inserts [30, 31, 34], and use of fins in electronic devices for extending the life of devices [28, 36]. Many researchers [27, 33, 35, 37, 39, 41] concentrated on space heating material for thermionic storage, while others [31] concentrated on nanoscale material fluid, such as air or water [26, 29, 30, 32, 36, 38], for transporting heat. The performance and emission characteristics of various bio-oils utilised as a source of electricity and power through engines were the subject of only a few of them, who concentrated on this topic.

2. Objective

The main goal is to investigate how different mass flow rates and axial velocities affect solar preheaters with intentionally roughened broken curved rib's ability of transmission of heat. Additionally, this will be done to find out how these variables affect heat transport. The remaining major objectives are divided as follows:

1. To determine the Nusselt no. for different insert spacings and different mass flow rates.
2. To calculate the friction factor for various insert spacings and Reynolds no.s.
3. To calculate Pressure, Drop at different insert spacings and mass flow rates.
4. To calculate the typical wall temperature for different insert spacings with varying mass flow rates.
5. To design a variety of forms to get the best mass flow rate for different insert spacings.

3.1 Governing Equation

Often, the behaviour of the flow is determined by the fundamental ideas of classical mechanics, which specify the preservation of mass and momentum. This is typically the case. The momentum and continuity equations are used to simulate the supposed steady, incompressible, turbulent flow in this section of the analysis. The momentum equation and the continuity equation can both be expressed as follows.

3.1.1 Continuity Equation

The law of conservation of mass is another term for the continuity equation, which is another name for this law. Test the flow of the fluid amidst locations 1 and 2. The disparity amidst intake and output is referred to as accumulation in the context of the total mass balance. The mass that goes in and comes out is the same if there is no storage. The previous equation, which claims that mass cannot be created or destroyed inside this tube, may be taken to be true as long as the flow does not alter over time. We can determine when the momentum is in equilibrium using the continuity and momentum equations. The continuity equation tells us if the amount of fluid that enters a certain volume either leaves or stays there, while the momentum equation tells us when the momentum is in equilibrium. The Navier-Stokes (N.S.) equation is another term for the momentum equations. Most of the time, flow is explained using mathematical equations. As required by the K-epsilon replica, the simulation is being run using the N.S. equations.

The equation for determining continuity looks like this:

$$\frac{\delta(\rho\bar{u})}{\delta x} + \frac{1}{r} \frac{\delta(\rho r\bar{v})}{\delta r} = 0 \quad (3.1)$$

3.2 Momentum Equation

3.2.1 Axial Component (Z-Component)

$$\rho\bar{v} \left[\frac{\delta\bar{u}}{\delta r} + \bar{u} \frac{\delta\bar{u}}{\delta x} \right] = \frac{\delta\bar{p}}{\delta x} + \frac{\delta}{\delta x} \left(\mu_{eff} \frac{\delta\bar{u}}{\delta x} \right) + \frac{1}{r} \frac{\delta}{\delta r} \left(\mu_{eff} \frac{\delta\bar{u}}{\delta r} \right) + \frac{\delta}{\delta x} \left(\mu_{eff} \frac{\delta\bar{u}}{\delta x} \right) + \frac{1}{r} \frac{\delta}{\delta r} \left(\mu_{eff} \frac{\delta\bar{u}}{\delta r} \right) \quad (3.2)$$

3.2.2 Radial Component (R-Component)

$$\rho \left[\bar{v} \frac{\delta\bar{v}}{\delta r} + \bar{u} \frac{\delta\bar{v}}{\delta x} \right] = -\frac{\delta\bar{p}}{\delta r} + \frac{\delta}{\delta x} \left(\mu_{eff} \frac{\delta\bar{v}}{\delta x} \right) + \frac{1}{r} \frac{\delta}{\delta r} \left(r\mu_{eff} \frac{\delta\bar{v}}{\delta r} \right) + \frac{\delta}{\delta x} \left(\mu_{eff} \frac{\delta\bar{v}}{\delta x} \right) + \frac{1}{r} \frac{\delta}{\delta r} \left(r\mu_{eff} \frac{\delta\bar{v}}{\delta r} \right) - 2\mu_{eff} \frac{\bar{v}}{r^2} + \rho \frac{\bar{w}^2}{r} \quad (3.3)$$

3.2.3 Tangential Component (θ-Component)

$$\rho \left[\bar{v} \frac{\delta\phi}{\delta r} + \bar{u} \frac{\delta\phi}{\delta x} \right] = \frac{\delta}{\delta x} \left[\mu_{eff} \frac{\delta\phi}{\delta x} \right] + \frac{1}{r} \frac{\delta}{\delta r} \left[r\mu_{eff} \frac{\delta\phi}{\delta r} \right] - \frac{2}{r} \frac{\delta}{\delta r} \left[\mu_{eff} \phi \right] \quad (3.4)$$

Here \bar{u} , \bar{v} and \bar{w} are the mean velocity components along z, r and θ directions respectively
 $\phi = r\bar{w}$.

and the variable

Net effective viscosity ,

$$\mu_{eff} = \mu_l + \mu_t \quad (3.5)$$

Here μ_l and μ_t stand for molecular or laminar viscosity and eddy or turbulent viscosity respectively. The fluid property is the molecular or laminar viscosity, and the flow property is the eddy or turbulent viscosity. By using dimensional analysis, the eddy viscosity μ_t can be expressed as,

$$\mu_t = \rho V_t l \quad (3.6)$$

Here V_t , is the turbulent velocity scale and l is the turbulent length scale was postulated by Prandtl and Kolmogorov and later adopted in the standard k-ε replica

$$l = \frac{\kappa^{3/2}}{\epsilon} \quad (3.7)$$

$$V_t \sim \sqrt{k}$$

(3.8) From the equation (3.6) the eddy viscosity is obtained and it is given by

$$\mu_t = \frac{\rho c \mu k^2}{\epsilon} \quad (3.9)$$

The replicating constant, C_μ in the eddy viscosity formulation, as shown in equation (3.10), is empirically tuned for the simple shear layer. The constant, C_μ is given by

$$C_\mu = \left[\frac{-k_1 k_2}{1 + 8k_2 \frac{k^2}{\epsilon^2} \left(\frac{\delta U_s}{\delta n} + \frac{U_s}{R_c} \right) \frac{U_s}{R_c}} \right] \quad (3.10)$$

In the equation (3.10), $U_s = \sqrt{\bar{u}^2 + \bar{v}^2}$ and R_c is the radius of curvature of the streamline concerned (Ψ constant).

3.3 The Turbulent Replicating

3.3.1 Kappa-Epsilon Replica

The K-epsilon replica is the one that is most usually used when attempting to describe the behaviour of turbulent flows. After being altered by Harlow and Nakayama and proposed by A.N. Kolmogorov, the K-Epsilon replica for turbulence was developed in 1942. The Realizable k-epsilon replica and the RNG k-epsilon replica are two examples of how the K-epsilon replica has been enhanced. The K-Epsilon Replica's transport equations are expressed in terms of k. The K-epsilon replica provides a solution to the issue under some unusual conditions. Only in conditions with a turbulent flow and a high Reynolds no. is the K-epsilon replica applicable.

K - EQUATION

$$\rho \left[u \frac{\partial k}{\partial x} + v \frac{\partial k}{\partial r} \right] = \frac{\partial}{\partial x} \left[(\mu_l + \frac{\mu_t}{\sigma_k}) \frac{\partial k}{\partial x} \right] + \frac{1}{r} \frac{\partial}{\partial r} \left[r (\mu_l + \frac{\mu_t}{\sigma_k}) \frac{\partial k}{\partial r} \right] + \rho g - \rho \epsilon \quad (3.11)$$

Where, G is the production term and is given by

$$\mu_t \left[2 \left\{ \left(\frac{\partial v}{\partial r} \right)^2 + \left(\frac{\partial u}{\partial x} \right)^2 + \left(\frac{v}{r} \right)^2 \right\} + \left(\frac{\partial u}{\partial r} + \frac{\partial v}{\partial x} \right)^2 \right] \quad (3.12)$$

the production term, which reflects the transfer of kinetic energy from the mean flow to turbulent motion, is created by the interaction amidst turbulent fluctuations and mean flow velocity gradients.

ε - EQUATION

$$\rho \left[\mu \frac{\partial \varepsilon}{\partial x} + \nu \frac{\partial \varepsilon}{\partial r} \right] = \frac{\partial}{\partial x} \left[(\mu_t + \frac{\mu}{\sigma_\varepsilon}) \frac{\partial \varepsilon}{\partial x} \right] + \frac{1}{r} \frac{\partial}{\partial r} \left[(r \mu_t + \frac{\mu}{\sigma_\varepsilon}) \frac{\partial \varepsilon}{\partial r} \right] + \frac{C_{s1}}{S_1} \frac{G \varepsilon}{k} - \frac{C_{s2}}{S_2} \frac{\varepsilon^2}{k} \quad (3.13)$$

Here C_{s1} , C_{s2} , σ_k and σ_ε are empirical turbulent constant. The values are considered according to the Launder, et. al.

3.4 Performance Parameters

We will talk about the features of the pressure drop and heat transfer in this section. Additionally, equations for calculating the pressure drop, heat transfer and efficiency, and dimensionless groups are presented. In the study Wang et al. conducted in 1996, the data from the graphs are shown after the explanations of the performance characteristics. In this investigation, the friction factor and the Reynolds no. were compared.

3.4.1 Dimensionless Group's

When grading and sizing heat exchangers, incorporate flow friction and characterise heat transfer. In this method of characterization, the pressure drop is defined and measured using the friction factor f and the Colburn factor j. The equation used to calculate the dimensionless groups used in this study is presented below, along with a brief explanation of how it was applied.

3.4.1.1 Reynolds No

The consistency of Reynold In fluid dynamics, the ratio of viscous force to inertial force is denoted by the sign "re." The dimension that represents the study's Reynold's no. characteristic is the tube collar diameter, denoted by Dc.

$$Re = \frac{\rho \cdot U_i \cdot D_h}{\mu} \quad (3.14)$$

3.4.1.2 Friction Factor (f)

Fanning friction factor is ratio of wall shear stress to flow kinetic energy. It is related to pressure drop tube heat exchangers as:

$$f = \frac{\Delta p \cdot \frac{D_h}{L_t}}{\frac{1}{2} \cdot \rho \cdot U_i^2} \quad (3.15)$$

Where L_t is length of duct,(m); ρ is air density (Kg/m^3); Δp is pressure drop (Pa).

3.4.1.3 Colburn j-Factor

Colburn j-factor is ratio of convection heat transfer (per unit duct surface area) to amount virtually transferable (per unit of cross-sectional flow area).

$$j = \frac{Nu}{Re \cdot Pr^{1/3} D_c} \quad (3.16)$$

3.4.1.4 Nusselt No. (Nu)

Nusselt no. is the ratio of convective conductance h to molecular thermionic conductance k/D_h .

$$Nu = \frac{h}{k / D_h} \quad (3.17)$$

Nusselt no. depends upon hydraulic diameter (D_h).

$$D_h = \frac{4(F_p - t)(P_t - D_c)P_l}{2(P_t P_l - \pi D_c^2 / 4) + \pi D_c (F_p - t)} \quad (3.18)$$

3.4.1.5 Prandtl No. Pr

Prandtl no. Pr is the ratio of a fluid's momentum diffusivity to thermionic diffusivity.

$$Pr = \frac{\nu}{\alpha} = \frac{\mu C_p}{k} \quad (3.19)$$

3.4.1.6 Pressure Drop

The extent of pumping power required for operating a heat exchanger is impacted by pressure dip that occurs. When it comes to design concerns, accurately characterizing the pressure drop is vital. The pressure drop in tube-and-fin heat exchangers may be represented mathematically using the following equations: This section begins with an investigation of the connection amidst the pressure dip and the pumping power, and then continues on to investigate the elements that contribute to the pressure dip:

$$\Delta p = \frac{L}{D} \frac{\rho V^2}{2} \quad (3.20)$$

Due to pressure dip in a heat exchanger (along with associated pressure dip in the in-out headers, nozzles, ducts, etc.) is proportional to the amount of fluid pumping power that is required for the heat exchanger to function, pumping power P is frequently seen as a significant design constraint. The following expression explains this relationship.

4.1 Numerical Solution

Fluid movement may be efficiently predicted using Computational Fluid Dynamics in a variety of situations, allowing for proper design. This is a result of the availability of numerical techniques and advancements in computer technology, which are to blame. Computational Fluid Dynamics technology is a cutting-edge approach for researching fluid flow dynamics and the processes of mass and heat transmission. Three-dimensional simulations of heat transfer characteristics are now achievable thanks to advancements in physical replicas, numerical analysis, and computing capacity. Recent research has allowed for this to be achievable. A 3-D approximation of a turbulent flow will be used for research since it is much more efficient than a two-dimensional approximation due to both its 3-D approach and the natural three-dimensionality of a turbulent flow. Unfortunately, due to the lengthy computation times needed to complete such studies, detailed study on fluid flow through three-dimensional pipes is not very common. As a result, replicating the three-dimensional flow field while taking into consideration the precise geometrical constraints looks to be a challenging task. The FLUENT computational fluid dynamics software package is used to identify the associated difficulties. For the finite volume technique to be used, the user is responsible for providing FLUENT with the grid system, the physical attributes, and the boundary conditions. Before simulating a problem, it is necessary to take into account basic computer replica concerns including boundary conditions, the size of the computational domain, grid topology, and two- or three-dimensional replicas. some fundamental computer. For example, selecting the best grid type could cut down on the setup and computing costs as well as time. The development of more successful results will be aided by selecting the suitable physical replicas and solution methodology. Depending on the work at hand, it is feasible that the size of the computational domain as well as the form, density, and smoothness of the cell surfaces will all need to be carefully considered while designing and meshing the geometry. FLUENT checks the grid once it has one before building replicas, boundary conditions, and material properties to get ready to solve the issue. FLUENT provides customers with the option to remedy the issue using the same approach if the grid doesn't need to be refined any longer. In this study, the effects of inefficient distribution on the solar pre-heater will be quantitatively analysed. Throughout the research phase, "ANSYS Fluent 15.0" was used as a programme. The computational fluid dynamics (CFD) software ANSYS Fluent 15.0 is used to replica fluid flow-related problems. The replicating approach for the three-dimensional computing operation used a tetrahedral mesh. All throughout the 3-D duct domain, the element sizes are fixed. A grid independence test was used to verify whether the accuracy of the solution's mesh quality had been preserved. Greater than 0.9%, which is regarded as the ideal mesh quality for computational purposes, of additional optimization did not alter the output.

4.2 Methodology

The four process flow steps that make up the current study's methodology are geometry replicating, pre-processing, processing, and post-processing. The following stages are part of the methodologies:

- A mathematical replica of the system is considered.
- The replica was created in SOLIDWORKS.

- Comparison to earlier research to validate the current work.
- Calculating the variables affecting heat transmission.
- Run the application to get the graphs with various parameter settings.
- Analysis of obtained plots by plotting.
- Enhancement of the system.

4.1. The dimension of air heater geometry parameters

Heater type	Solar preheater having broken arc rib
Length	640 mm
Width	100 mm
Hight	20 mm
Arc angle (α)	30
Comparitive roughness pitch (p/e)	8 to 14
Comparitive roughness height (e/Dh)	0.045
Gap width (g/e)	1
Fluid	Air

4.3 Simulation of Flow Through Solar Preheater

FOR CFD REPLICATING OF SOLAR PREHEATER AT FIRST, SOLID WORKS UTILISED. DUE OF THIS, THE FLUID domain MIGHT BE CREATED. APPLICATION OF THE CHANNEL BOUNDARY CONDI-TIONS, FORMULATION OF HYPOTHESES, USE OF EQUATIONS, COMPUTATION OF THE FINDINGS, AND ANALYSIS OF THE RESULTS WERE ALL FINISHED.

4.4 Geometrical Description

SOLAR PREHEATER'S GEOMETRY WAS BUILT USING SOLID WORKS 2013, WHICH WAS THEN USED TO SIMULATE HOW THE FLUID WOULD ACTIVATE IF IT WERE CONFINED INSIDE A CHANNEL. THE VARIATIONS OF THE HEATER WERE OBSERVED USING A SHAPE THAT RESEMBLED A CORRUGATED SHEET. MANY PLATE SHAPE REPLICAS ARE USED TO EXAMINE HOW VAR-IATIONS IN REYNOLDS No. AFFECT THE

EFFICIENCY OF HEATERS.

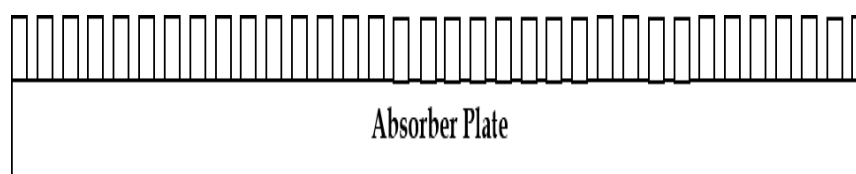
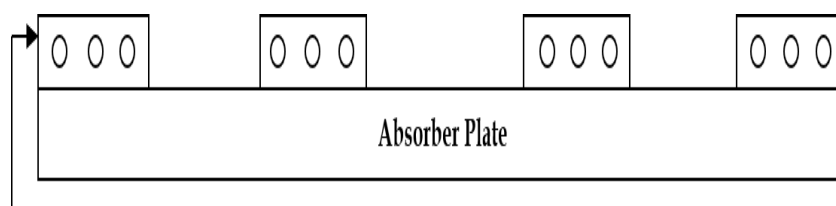


Figure 4.1. Side View of Absorber Plate having Perforated Curve Ribs



Perforated Curve Ribs

Figure 4.2. *Side View of Absorber Plate having Perforated Curve Ribs*

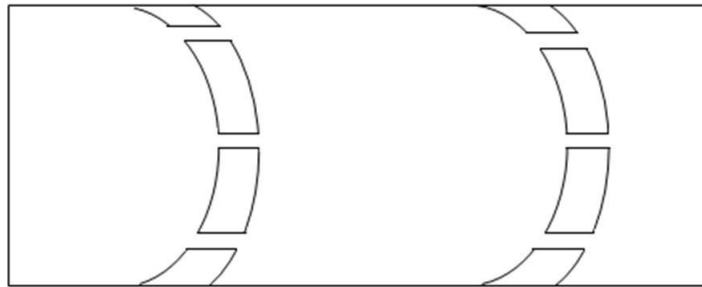


Figure 4.3. *Top View of Absorber Plate having Perforated Curve Ribs*

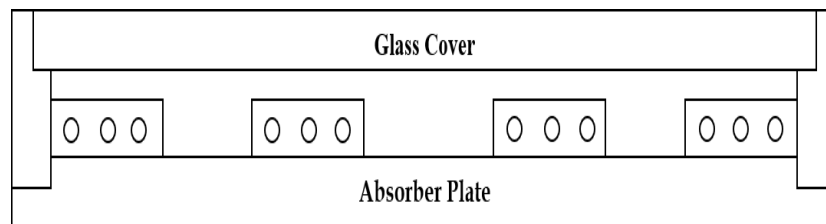


Figure 4.4. *Front View of Solar Air Heater with Absorber Plate having Perforated Curve Ribs*

5. Result and Discussion

In the present study, the efficiency of solar preheaters is examined in relation to their effectiveness. Both basic solar preheaters and those with the shape of three intersecting triangles inside tubes are subjected to analysis. In ANSYS Fluent 15 programme, CFD analysis was performed on both designs. The differences amidst multiple turbulence replicas can thus be evaluated and compared in this manner. By examining how the Nusselt no. and the Reynolds no, which are relevant to both designs, are related, the turbulence replica is chosen. The regular K-replica, the K-replica RNG, and the K-replica realisable replica are all applied to validate the results. For both designs, Nusselt no. in Dittus-Boelter equation. They are contrasting a no. of turbulence replicas before choosing the K-turbulence RNG replica to be used for the analysis of the current research. The most recent numerical findings agree with those previously made. As a result, the recently calculated finding and earlier discoveries are reasonably consistent with one another.

5.1 Validation of Model

Efficiency of solar preheaters is being investigated in the current study. Analysis is done on both simple solar preheaters and those with the shape of three intersecting triangles inside tubes. ANSYS Fluent 15 was used to conduct a CFD analysis on both designs.

Test for grid independence, has been done as shown in figure 5.1. For a variety of Reynolds no.s, multiple mesh element counts (265131, 871997, 1508485, and 2080414) are carried out in order to determine the Russell no. for a smooth duct. The Russell no. exhibits an early increasing trend, but after the mesh element 1508485, its value starts to level out.

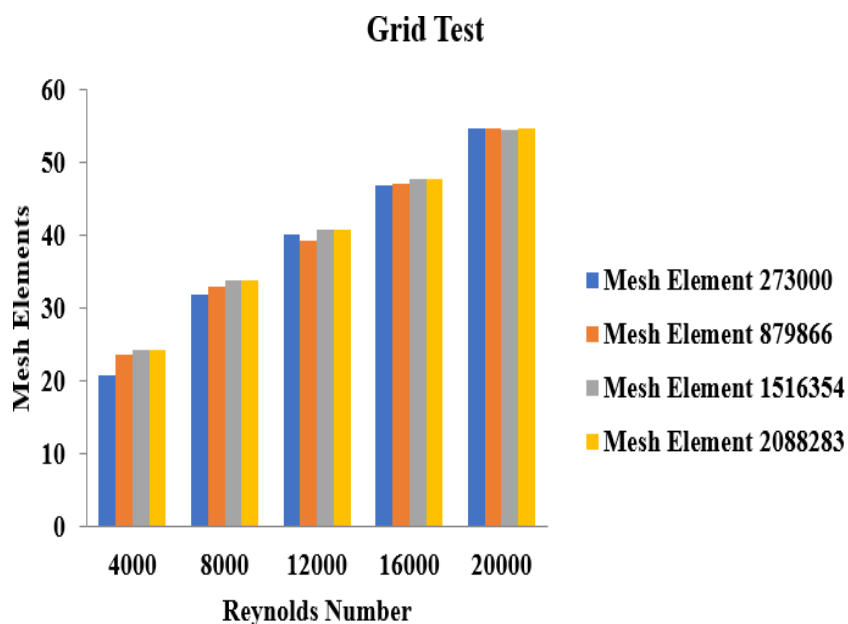


Fig .5.1. *Nusselt and Reynolds no. for different mesh element*

5.1.2. Selection of replica

We used the Dittus-Boelter equation together with a no. of various turbulence replicas and compared them in order to select one that was appropriate for a smooth duct. The experiment's findings are displayed in Figure 5.2. The choice of turbulence replicas in both designs is based on how the Nusselt no. and the Reynolds no. relate to one another. The K-replica standard, K-replica realisable replica, and K-replica random no. generator are used to verify the results. The Nusselt no. of the Dittus-Belter equation is employed in the formulation and analysis of the equation. Since several turbulence replicas have been compared to the dit-tus K-turbulence RNG replica, which produces better results, it is almost being studied in this current endeavour. The purpose of this comparison was to ascertain whether This comparison was done to ascertain whether or not this replica provides the greatest outcomes as shown in figure 5.2.

The results range from 2.4% to 9.6% when the friction factor of a smooth duct is calculated using the modified Blasius equation and the results are compared to the CFD findings presented in fig. 5.3. This shows that a variety of elements can lower a smooth duct's friction factor.

5.2 Effect of comparative roughness pitch

Reynolds no.s amidst 4000 and 20000 are influenced by friction factor and Nusselt no. The comparative roughness pitch has an impact on this. No matter whether convection is present or not, it is generally known that roughened ducts have a significantly higher heat transfer coefficient than smooth ducts. The image supports this phenomenon and provides additional proof that it occurs. This phenomenon is the result of mixing and flow separation caused by the creation of eddies in the wake zone of each rib. The effective roughness pitch must be specified at a P/e value of 10. The development of a boundary layer with minimal heat transport results in a shift in the Nusselt no. as shown in figure 5.4.

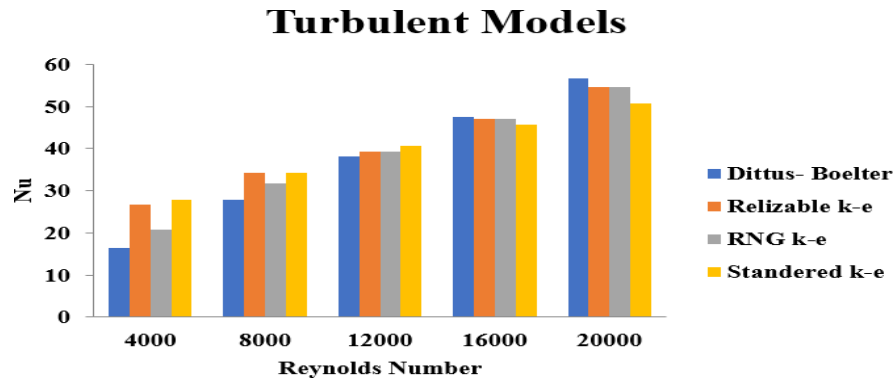


Fig. 5.2. Reynolds no. and Nusselt no. for different turbulent replica.

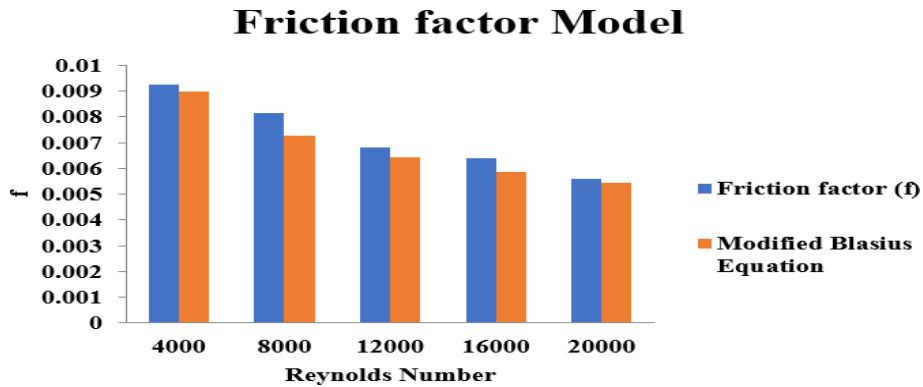


Fig. 5.3. Friction factor .and Reynolds no. cfd & modified blasius equation

5.3 Effect on Arc angle

Changes in Nusselt no. at various Reynolds no. values and in relation to the angle of attack. At 30 degrees, 45 degrees, 60 degrees, and 75 degrees, Reynolds no. rises like Nusselt no. Its assault angle is the largest one that can be achieved and is 30 degrees higher than this valley of attack. For different Reynolds no.s, Nusselt no. declines as shown in figure 5.5. From figure 5.6 it is clearly understood that at p/e ratio 10 thermal performance of preheater of broken perforated curve ribs are coming better than other p/e ratio at Re range upto 12000 but p/e ratio 14 are coming better for Re range 12000 to 20000.

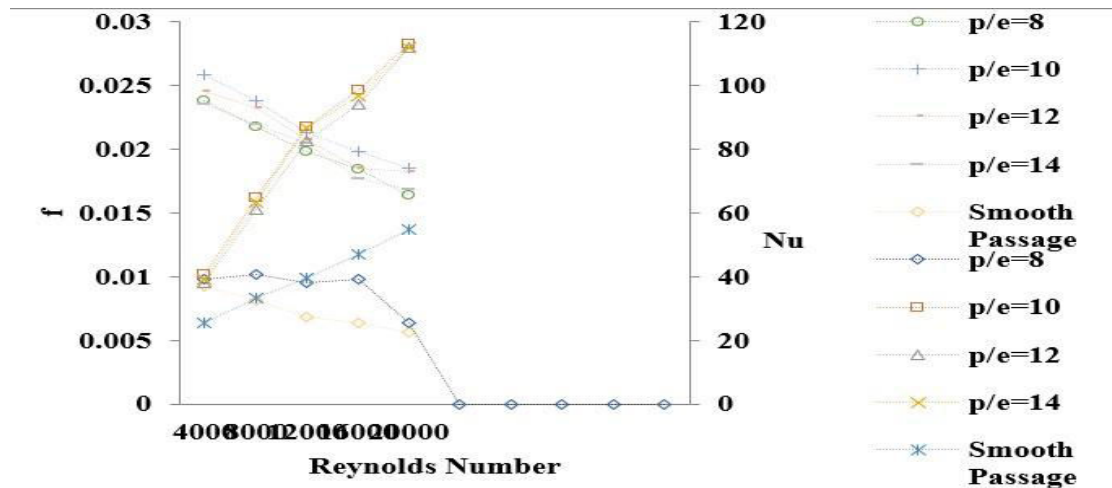


Fig .5.4. Nusselt No. Vs Friction Factor and Reynolds no. at different roughness pitch

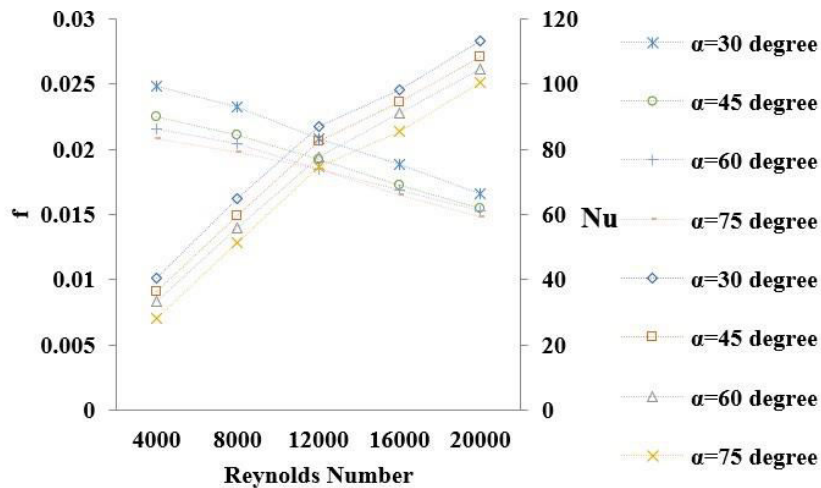


Fig 5.5. Nussely No. Friction Factor and Reynolds no. with different curve pitch

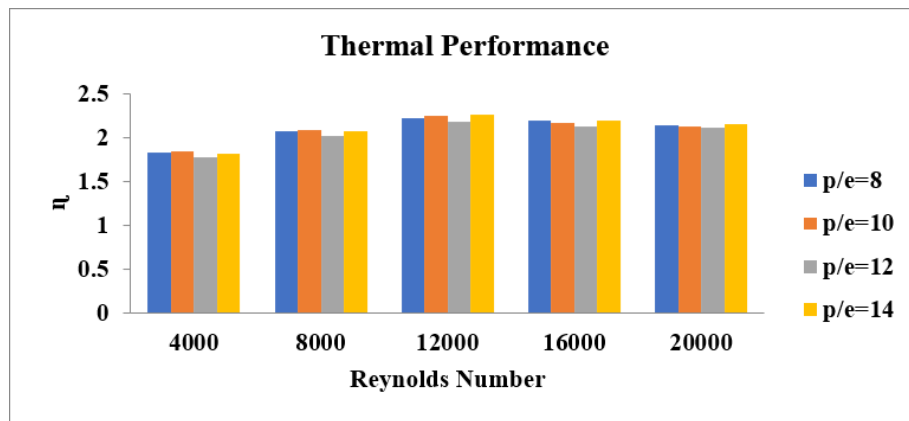


Fig.5.6. Thermohydraulic performance and Reynolds no.

Conclusion

The impact of arranging arc-shaped ribs in a broken curved rib pattern on one of the wide sides of a solar preheater duct was examined in this computational fluid dynamics study. The task was carried out using Ansys Fluent 15.0. To ascertain their impacts on friction factor and heat transmission, the comparative roughness height (e/D_h), comparative roughness height (p/e), and comparative roughness width (W/w) have all been examined (Nusselt no.). The findings of the investigation led to the conclusions detailed below.

For all feasible values of roughness pitch, the standard Nusselt no. rises as Reynolds no. rises.

As Reynolds no. varies for different levels of roughness pitch, the standard friction factor declines.

Reynolds no. stays constant as the arc angle increases, but standard Nusselt no.

decreases.

When the roughness pitch (p/e) was 10 and the roughness height (e/D_h) was 0.045, it was found that the maximum Nusselt no. was 2.2524 times higher than that of a smooth duct at a Reynolds no. of 12000. This was true that roughness pitch (p/e) measurement was made.

Significance of thermohydraulic performance (ν) varies amidst 1.1851 and 1.6267 when the arc angle is set to 30 degrees, the roughness pitch is set to 10 (p/e), the roughness height is set to 0.045 (e/D_h), and the Reynolds no. is amidst 4000 and 20000.

Ideal value of thermo-hydraulic performance at a Reynolds no. of 12000 is 1.6267 when the roughness pitch (p/e), roughness height (e/D_h), and arc angle are all 10.

References

- V.S. Hans, R.S. Gill, Sukhmeet Singh, "Heat transfer and friction factor correlations for a solar preheater duct roughened unnaturally with broken arc ribs" (2016).
- Tabish alam, "Numerical study on thermionic hydraulic performance enhancement in solar preheater duct with semi ellipse shaped obstacles" (2015).
- Tabish alam, "A critical review on unnatural roughness provided in rectangular solar preheater duct" (2013)
- Deep Singh Thakur, Mohd. Kaleem Khan, ManabendraPathak, "Performance Evaluation of Solar preheater with Novel Hyperbolic Rib Geometry" (2015).
- Amit Kumar Ahuja, J. L. Bhagoria "A CFD based Thermo-Hydraulic Performance Analysis of an Unnaturally Roughened Solar preheater Having Circular Ribs on the Absorber Plate" n (2015).
- N.K. Pandey, V.K. Bajpai, Varun "Experimental investigation of heat transfer augmentation using multiple arcs with gap on absorber plate of solar preheater" (2016).
- Yadav A.S., Bhagoria J.L., "A CFD based heat transfer and fluid flow analysis of a solar preheater provided with circular transverse wire rib roughness on the absorber plate", *Energy*, Vol. 55, pp. 1127 – 1142, (2013).
- Raj Kumar et al. "Study and correlation development correlation for Nusselt no. and friction factor for discredited broken V-pattern baffle solar air channel"
- Karwa R., Solanki, S. C. and Saini, J. S., "Heat transfer coefficient and friction factor correlations for the transitional flow regime in rib-roughened rectangular ducts", *International Journal of Heat and Mass Transfer*" 1999.
- Sukhatme K. and Sukhatme S. P., 1996, "Solar energy: principles of thermionic collection and storage, Tata McGraw-Hill Education".
- Cengel Y. A. and Cimbala J. M., 2006, "Fluid mechanics (Vol. 1), Tata McGraw-Hill Education".
- Yadav A. S. and Bhagoria J. L., "Heat transfer and fluid flow analysis of solar preheater: a review of CFD approach", *Renewable and Sustainable Energy Reviews*, 2013
- Kumar A., Bhagoria, J. L. and Sarviya R. M., "Heat transfer and friction correlations for unnaturally roughened solar preheater duct with discrete W-shaped ribs", *Energy Conversion and Management* 2009,
- Khushmeet Kumar, D.R. Prajapati, Sushant Samir, Investigation on Heat Transfer and Friction Factor Correlations Development for Solar preheater Duct Unnaturally Roughened with 'S' Shape Ribs
- R.S. Gill, V.S. Hans, J.S. Saini, Sukhmeet Singh, Investigation on performance enhancement due to staggered piece in a broken arc rib roughened solar preheater duct, *Renewable Energy* (2016), doi: 10.1016/j.renene.2016.12.002
- Yadav and Bhagoria "A CFD base heat transfer and fluid flow analysis of a solar preheater provided with circular transverse wire rib roughness on the absorber plate." *Renewable energy*, 2013
- A review on Solar preheater using various unnatural roughness geometries Ankit C. Khandelwal, 2Samir A.Dhatkar, 3A.B.Kanas-Pat
- Deep Singh Thakur, Mohd. Kaleem Khan, Manabendra Pathak, Performance Evaluation of

- Solar preheater with Novel Hyperbolic Rib Geometry, *Renewable Energy* (2016), doi: 10.1016/j.renene.2016.12.092
- Jaurker, A.R. Saini, J.S. and Gandhi, B.K., "Heat transfer and friction characteristics of rectangular solar preheater duct using rib-grooved unnatural roughness", *Solar Energy*, 80, pp. 895 – 907, (2006).
- Karmare, S.V. and Tikekar, A.N., (2007). Heat transfer and friction factor correlation for unnaturally roughened duct with metal grit ribs, *Int. Journal of Heat Mass Transfer*, 50, pp. 4342 – 4351.
- Karwa, R. Solanki, S.C. and Saini, J.S., (1999) Heat transfer coefficient and friction factor correlations for the transitional flow regimes in rib-roughened rectangular duct, *Int. Journal of Heat Mass Transfer*
- T. Alam, R.P. Saini, J.S. Saini, Use of turbulators for heat transfer augmentation in an air 15 duct – a review, *Renewable Energy*, 62 (2014), pp. 689–715
- Aharwal, Gandhi and Saini "Heat transfer and friction characteristics of solar preheater ducts having integral inclined discrete ribs on absorber plate" *Heat and mass transfer* (2009).
- Langewar, Bhagoria and Agrawal "Review of development of unnatural roughness in solar preheater and performance evaluation of different orientations for double arc rib roughness"
- Singh A.P., Varun, Siddhartha, (2014), "Effect of unnatural roughness on heat transfer and friction characteristics having multiple arc shaped roughness element on the absorber plate", *Solar Energy*, Vol. 105, pp. 479 – 493.
- Neeraj Bisht, P. C. Gope, Kuldeep Panwar, Influence of crack offset distance on the interaction of multiple cracks on the same side in a rectangular plate, *Frattura ed Integrità Strutturale*, 32 (2015) 1-12; DOI: 10.3221/IGF-ESIS.32.01.
- Kuldeep Panwara, D.S. Murthy, Design and Evaluation of Pebble Bed Regenerator with Small Particles, *Materials Today: Proceedings 3* (2016) 3784–3791.
- Shivasheesh Kaushik, Vinay Sati, Nikhil Kanojia, Kuber Singh Mehra, Himanshu Malkani, Harshvardhan Pant, Hina Gupta, Abhay Pratap Singh, Aman Kumar, Ashwarya Raj Paul, and Ritu Kumari, 2021. Bio-Diesel a Substitution for Conventional Diesel Fuel: A Comprehensive Review, *Lecture Notes in Mechanical Engineering*, Springer Nature Singapore, <https://doi.org/10.1007/978-981-16-0942-8>, 113-122.
- Shivasheesh Kaushik, Satyendra Singh, 2019, Analysis on Heat Transmission and Fluid Flow Attributes in Solar Air Accumulator Passage with Diverse Faux Jaggedness Silhouettes on Absorber Panel, *International Journal of Engineering and Advanced Technology*, 8, 32-41.
- Kaushik, S., Singh, S., Kanojia, N., Rawat, K. and Panwar, K., 2020. Comparative Study for Thermionic and Fluid Flow Peculiarities in Cascading Spiral Inner Tube Heat Exchanger with or without Diverse Inserts over Spiral Tube, *IOP Conf. Series: Materials Science and Engineering 802*, doi:10.1088/1757-899X/802/1/012009.
- Kaushik, S., Singh, S., and Panwar, K., 2021. Comparative Study for Thermionic and Fluid Flow Peculiarities in Cascading Spiral Inner Tube Heat Exchanger with or without Diverse Inserts over Spiral Tube Comparative analysis of thermionic and fluid flow behaviour of diverse nano fluid using Al₂O₃, ZnO, CuO nano materials in concentric spiral tube heat exchanger, *Materials Today: Proceeding*, doi: <https://doi.org/10.1016/j.matpr.2021.04.100>, 6625-6630.
- Kaushik, S., Singh, S., and Kanojia, N., Naudiyal R., Kshetri R., Paul A. R., Kumari R., Kumar A. and Kumar S., 2020. Effect of introducing varying no. of fins over LED light bulb on thermionic behaviour, *Materials Today: Proceeding*, doi: <https://doi.org/10.1016/j.matpr.2020.10.876>, 9794- 9799.
- Kanojia, N., Kaushik, S., Panwar, K., Kshetri R., and Singh, M., 2020. Experimental investigation of optimum charging and discharging time on packed bed heat regenerator for space heating and solar drying application, *Materials Today Proceeding*, doi: <https://doi.org/10.1016/j.matpr.2021.04.210>, 2214-7853, 6612-6618.
- Uniyal, V., Joshi, S. K., Kaushik, S., and Kanojia, N., 2020. CFD Investigation of Transfer of

- the Heat and Turbulent Flow in Circular Copper Tube with Perforated Conical Rings of Aluminum Material, *Materials Today: Proceeding*, doi: <https://doi.org/10.1016/j.matpr.2021.04.217>, 6619-6625.
- Nikhil Kanojia, Shivasheesh Kaushik, Vipin Uniyal, Kuldeep Panwar, Satyendra Singh, Shubham Singh Karki, Samridhhi Vashishth, Anurag Rawat, Ashish Nayal, 2022. Experimental Study of Heat Storage and Heat Elimination in Packed Bed using Nylon 6 Spiral Balls, *Neuro Quantology*, Vol. 20, Pages 2335-2343
- Ayushman Shrivastav, Shivasheesh Kaushik, Kuldeep Rawat, Abhishek Ghildyal, Vijay Singh Bisht, Kamal Rawat, Prabhakar Bhandari 2022. Influence of M shaped, Wedge shaped and Reverse Wedge shaped Turbulators in Solar preheater, *Neuro Quantology*, Vol. 20, Pages 2308-2312
- Nikhil Kanojia, Shivasheesh Kaushik, Subhan Ali, Ashish Joshi, Satyendra Singh, Aman Kumar, Bashishtha Kumar Rewani, Prince Kumar Gupta, Sahwaj Alam, 2022. Review on Sustainable Thermionic Energy Storage Technology with Packed Bed Regenerator, *Neuro Quantology*, Vol. 20, Pages 2324-2334
- Ayushman Shrivastav, Shivasheesh Kaushik, Kuldeep Rawat, Jaya Bohra, Vijay Singh Bisht, Prabhakar Bhandari, Kamal Rawat 2022. Exergy Analysis of Solar preheater roughened with Z-Shaped Baffles , *Neuro Quantology*, Vol. 20, Pages 2313-2317.
- Kuldeep Rawat, Avinash Singh, Krishna Sati, Manish Kumar, Ashish Negi, Kuldeep Panwar, 2021. CFD analysis of fixed matrix with glass refractory particle regenerator, *Materials Today: Proceedings*, Volume 46, Part 15, Pages 6871-6875, <https://doi.org/10.1016/j.matpr.2021.04.450>.
- Panwar, K., Hasan, E., Singh, R., Chaudhary, V., Rawat, K. 2019. Thermionic and Resistance Analysis of Perforated Fin Using CFD, *Advances in Fluid and Thermionic Engineering. Lecture Notes in Mechanical Engineering*. Springer, Singapore. https://doi.org/10.1007/978-981-13-6416-7_56
- Nikhil Kanojia, Shivasheesh Kaushik, Mayank Singh, Manish Kumar Sha, 2021. A Comprehensive Review on Packed Bed Thermionic Energy Storage System, *Lecture Notes in Mechanical Engineering*, Springer Nature Singapore, <https://doi.org/10.1007/978-981-16-0942-8>, 165-174.
- Shivasheesh Kaushik, Ashish Joshi, Nikhil Kanojia, Subhan Ali, Avinash Guleria, Aman Thakur, Mohit Nayal, Yash Khandsaliya, 2022. Comparative Analysis of Physio-Chemical, Performance-E Emission Properties Amidst Diesel and varying blend of Castor Biodiesel with Iso-Propanol, *Neuro Quantology*, Vol.20, 2272-2285.
- Shivasheesh Kaushik, Subhan Ali, Ashish Joshi, Kuldeep Panwar, Ashish Benwal, Arshad Khan, Dheeraj Kumar, Divyanshu Kumar, 2022. Experimental Analysis of Performance and Emission Characteristic amidst Diesel and Varying Blends of diesel-Isopropanol-Biogas with different CR, *Neuro Quantology*, Vol.20, 2272-2285. 2286-2307.